HHS Public Access

Author manuscript

Mech Dev. Author manuscript; available in PMC 2016 November 01.

Published in final edited form as:

Mech Dev. 2015 November ; 138 Pt 3: 279–290. doi:10.1016/j.mod.2015.10.001.

A role of *glypican4* and *wnt5b* in chondrocyte stacking underlying craniofacial cartilage morphogenesis

Barbara E. Sisson[1,2], **Rodney M. Dale**[1,3], **Stephanie R. Mui**[1], **Jolanta M. Topczewska**[1,4], and **Jacek Topczewski**[1]

[1]Northwestern University Feinberg School of Medicine, Department of Pediatrics, Stanley Manne Children's Research Institute, Chicago, IL 60611, USA

[2]Ripon College, Department of Biology, Ripon, WI 54971, USA

[3]Loyola University Chicago, Department of Biology, Chicago, IL 60660, USA

[4]Northwestern University Feinberg School of Medicine, Department of Surgery, Stanley Manne Children's Research Institute, Chicago, IL 60611, USA

Abstract

The Wnt/Planar Cell Polarity (PCP) pathway controls cell morphology and behavior during animal development. Several zebrafish mutants were identified as having perturbed Wnt/PCP signaling. Many of these mutants have defects in craniofacial formation. To better understand the role that Wnt/PCP plays in craniofacial development we set out to identify which of the mutants, known to be associated with the Wnt/PCP pathway, perturb head cartilage formation by disrupting chondrocyte morphology. Here we demonstrate that while *vang-like 2* (*vangl2), wnt11* and *scribbled (scrib)* mutants have severe craniofacial morphogenesis defects they do not display the chondrocyte stacking and intercalation problems seen in *glypican 4* (*gpc4*) and *wnt5b* mutants. The function of Gpc4 or Wnt5b appears to be important for chondrocyte organization, as the neural crest in both mutants is specified, undergoes migration, and differentiates into the same number of cells to compose the craniofacial cartilage elements. We demonstrate that Gpc4 activity is required cell autonomously in the chondrocytes and that the phenotype of single heterozygous mutants is slightly enhanced in embryos double heterozygous for *wnt5b* and *gpc4*. This data suggests a novel mechanism for Wnt5b and Gpc4 regulation of chondrocyte behavior that is

Correspondence to: Jacek Topczewski.

Barbara E. Sisson, 300 Seward St., Ripon College, Ripon, WI 54971, sissonb@ripon.edu
Rodney M. Dale, Loyola University Chicago, Quinlan 222, 1032 W. Sheridan Rd., Chicago, IL 60660, rdale1@luc.edu
Stephanie R. Mui, Department of Pediatrics, Northwestern University Feinberg School of Medicine, Stanley Manne Children's Research Institute, 225 East Chicago Avenue, Box 204, Chicago, Illinois 60611-2605, stephanie.r.mui@gmail.com
Jolanta M. Topczewska, Department of Surgery, Northwestern University Feinberg School of Medicine, Stanley Manne Children's Research Institute, 225 East Chicago Avenue, Box 93, Chicago, Illinois 60611-2605, j-topczewska@northwestern.edu
Jacek Topczewski, Department of Pediatrics, Northwestern University Feinberg School of Medicine, Stanley Manne Children's Research Institute, 225 East Chicago Avenue, Box 204, Chicago, Illinois 60611-2605, j-topczewski@northwestern.edu, Phone number: (773) 755-6545

independent of the core Wnt/PCP molecules and differs from their collaborative action of controlling cell movements during gastrulation.

Keywords

Wnt/PCP pathway; *knypek*; *pipe tail*; growth plate

1. Introduction

The Wnt/Planar Cell Polarity (PCP) pathway, initially identified in *Drosophila* (Gubb and Garcia-Bellido, 1982), plays an important role in patterning the polarity of epithelial and mesenchymal cells in invertebrates and vertebrates. In zebrafish, this pathway is particularly linked to convergence and extension cell movements during gastrulation (Heisenberg et al., 2000; Jessen et al., 2002; Park and Moon, 2002; Rauch et al., 1997; Topczewski et al., 2001; Wada et al., 2005) and neuronal migration (Wada et al., 2005; Wada and Okamoto, 2009). The pathway also regulates aspects of zebrafish organogenesis (Dale et al., 2009) such as establishing hair cell polarity within the neuromasts of the lateral line, the sensory system, of the zebrafish (Lopez-Schier and Hudspeth, 2006; Lopez-Schier et al., 2004). In addition, two of the mutants that exhibit convergence and extension defects, *glypican 4 (gpc4; knypek)* and *wnt5b (pipe tail)*, also have shortened craniofacial cartilage elements (Hammerschmidt et al., 1996; LeClair et al., 2009; Piotrowski et al., 1996; Solnica-Krezel et al., 1996; Topczewski et al., 2001).

Craniofacial cartilage elements are derived from the cranial neural crest. In zebrafish, Wnt/PCP signaling plays a role in the migration of the cranial neural crest (De Calisto et al., 2005). As neural crest cells migrate they extend polarized protrusions allowing the cells to migrate in a directed motion. The polarization of these protrusions is controlled in part by Wnt/PCP elements Wnt11, Fzd7 and Disheveled (Carmona-Fontaine et al., 2008; Clay and Halloran, 2011; Matthews et al., 2008). The cranial neural crest cells migrate in four distinct streams, (1) premandibular, (2) mandibular (3) hyoid and (4) branchial. These streams then form the seven pharyngeal arches, with the third stream forming three of these arches (Knight and Schilling, 2006; Schilling et al., 1996). Following migration, the neural crest cells condense and begin to form the craniofacial cartilage elements. At the early larval stage, ~3.5 mm standard length (SL), the bones of the viscerocranium begin to form through either .endochondrial ossification of the cartilage elements (eg. hyosymplectic) or directly by membranous ossification around cartilage elements e.g. Meckel's cartilage) or without a cartilage mold (e.g. branchiostegal ray) (Cubbage and Mabee, 1996; Parichy et al., 2009).

The cartilage elements of *gpc4* and *wnt5b* mutants are shorter and built of rounded chondrocytes that do not stack properly (Hammerschmidt et al., 1996; Piotrowski et al., 1996; Solnica-Krezel et al., 1996; Topczewski et al., 2001). The morphology of the chondrocyte stacking defects in the *gpc4* and *wnt5b* mutant cartilages are similar to the defects found in the axial mesoderm of Wnt/PCP mutants during gastrulation (Glickman et al., 2003; Lin et al., 2005) suggesting a role of the pathway in cartilage morphogenesis. Furthermore, rescued adult *gpc4*^{m818} mutants have smaller skulls and display a lack of

elongated cartilage in the palaquadrate elements (LeClair et al., 2009). While *gpc4* and *wnt5b* mutants exhibit shortened cartilage elements, they are not the only core PCP pathway members reported to display craniofacial skeleton defects. The zebrafish *wnt11* mutant *(silberblick)* also have smaller craniofacial cartilage, particularly in the jaw (Heisenberg et al., 1996) and embryos mutant for *vang-like 2 (vangl2; trilobite)* exhibit cyclopia and have a smaller head (Marlow et al., 1998).

Due to their role in convergence and extension and the similar body phenotypes found in *gpc4* and *wnt5b* mutants compared to other mutants disrupting core members of the PCP pathway, one might assume that all of the core genes of the Wnt/PCP pathway play a similar role in the morphogenesis of craniofacial cartilage. This hypothesis has yet to be tested. Here we explore the craniofacial cartilage phenotypes of members of the Wnt/PCP pathway within the zebrafish: *gpc4, wnt5b, wnt11, scrib (scribble1;llk),* and *vangl2*. We demonstrate that roles of Wnt11, Scrib or Vangl2 are in contrast with Gpc4 and Wnt5b which are required for the proper elongation of cartilage elements by regulating the process of chondrocyte elongation and stacking. This defect is not due to improper neural crest specification or migration, or a decrease in cell number. Furthermore, we show that Gpc4, acts cell autonomously in the control of cartilage morphogenesis and that *wnt5b* can enhance the cartilage phenotype of *gpc4* heterozygotes. Taken together these results suggest that Wnt5b and Gpc4 are specifically required for normal chondrocyte stacking.

2. 2. Results

2.1 Genes involved in the Wnt/PCP signaling pathway are expressed in the pharyngeal arches

As craniofacial cartilage phenotypes are observed in mutants of the PCP pathway, we sought to verify that these genes were expressed in the craniofacial cartilage during chondrocyte condensation and stacking (55 hours post fertilization (hpf) and 3 days post fertilization (dpf), respectively). Whole mount *in situ* hybridizations were performed on 55 hpf and 3 dpf embryos with probes for *vangl1, vangl2, gpc4, wnt5b, and wnt11* (Fig. 1). As expected, of the Wnt/PCP genes with known craniofacial defects, all were expressed in the pharyngeal arches (Fig. 1A–H', K–L') except *vangl1* (Jessen and Solnica-Krezel, 2004) (Fig. 1A–B'). Furthermore, *wnt5b* maintains its expression in the pharyngeal arches in $gpc4^{fr6}$ mutants (Fig. 1I–J'). Given the craniofacial phenotypes observed in *gpc4* and *wnt5b* mutants, we wanted to specifically observe the expression pattern of these genes within the pharyngeal arches at 55 hpf when the cartilage is still condensing. Whole mount *in situ* hybridizations for *gpc4* and *wnt5b* were performed on 55 hpf wild type embryos and cyrosectioned (Fig. 1N, O). To provide a reference for the location of the neural crest at this time point Sox10:GFP embryos, which express GFP in the neural crest, were also sectioned (Fig. 1P). This demonstrates that while *gpc4* is expressed in the pharyngeal endoderm, neural crest and mesoderm at 55 hpf, *wnt5b* has a more restricted pattern and is only expressed in the neural crest and mesoderm. Whole mount *in situ* hybridizations for *vangl2* were also performed (Fig. 1M) demonstrating that *vangl2* is expressed in the neural crest and mesoderm at 55 hpf.

2.2 Of the characterized zebrafish Wnt/PCP mutants, gpc4 and wnt5b are the only members to display a craniofacial cartilage stacking defect

While many of the zebrafish mutants in the Wnt/PCP pathway were first identified by their early convergence and extension phenotype of a shorter and broader body axis, many of the mutants also displayed craniofacial malformations, such as a shorter lower jaw and a reduced distance between the eyes (Heisenberg et al., 1996; Piotrowski et al., 1996; Solnica-Krezel et al., 1996). As these external cranial phenotypic features are morphologically linked due to their close proximity, they could be caused by several different defects that may affect one or both of these tissues. To determine if the identified mutants in the core Wnt/PCP genes generate these external phenotypes through similar processes, we characterized the underlying chondrocyte organization in these core Wnt/PCP mutants.

By 4 dpf most of the craniofacial cartilage elements of the zebrafish have formed (Kimmel et al., 1998) and have a very stereotypic shape between individuals. At this time the chondrocytes of the first and second pharyngeal arch elements, such as the symplectic, ceratohyal, and parts of Meckel's cartilage, show the characteristic "stack of pennies" organization in which thin and elongated chondrocytes are assembled on top of one another to form their respective cartilage element (Fig. 2A) (Kimmel et al., 1998). We examined the craniofacial cartilage elements of 4 dpf *wnt11*, *wnt5b*, *vangl2*, *scrib*, and *gpc4* mutants and their wild type siblings that were stained with Wheat Germ Agglutinin (WGA), which binds to N-acetyl-D-glucosamine in the cartilage extracellular matrix. This technique marks the outline of chondrocytes, which allowed us to assess the gross morphology of the cartilage elements as well as the dimensions of individual chondrocytes that comprise the cartilage using laser confocal microscopy (Fig. 2). In all of the mutants, many of the cartilage elements, especially the ceratohyal and Meckel's cartilage, were greatly deformed (Fig. 2B–F) when compared to wild type siblings as had been previously observed (Heisenberg et al., 1996; Piotrowski et al., 1996; Solnica-Krezel et al., 1996) (Fig. 2A). Interestingly, while the Wnt/PCP mutants do have similar morphological defects in overall cartilage structure we observed there seem to be different structural reasons for these variations.

Two Wnt ligands that are known to play a key role in the Wnt/PCP pathway are Wnt11 and Wnt5b (Heisenberg et al., 2000; Kilian et al., 2003; Rauch et al., 1997; Topczewski et al., 2001). Both *wnt11* and *wnt5b* mutants were identified in the 1996 zebrafish mutagenesis screen and categorized to have jaw and branchial arch phenotype (Fig. 2B–C) (Heisenberg et al., 1996; Piotrowski et al., 1996). While this is true, the *wnt11* mutant was primarily assigned to have a forebrain defect that causes the eyes to fuse due to the failure of the midline to bisect the eye field early during development whereas the *wnt5b* mutant was categorized due to its early convergence and extension defect during gastrulation. Examination of the *wnt11* mutant (Fig. 2B) revealed disrupted placement of many of the cartilage elements derived from the premandibular, mandibular, and the hyoid arches. However, the stacking of the chondrocytes seemed normal. In the *wnt5b* mutant (Fig. 2C) the placement of the cartilages was normal, but the cartilages were shorter and composed of rounded cells throughout the elements.

Interestingly, the *wnt11* eye phenotype can vary from animal to animal along with the severity of the craniofacial defects. To determine if the severity of the eye phenotype was correlated with the cartilage placement phenotype we looked at embryos manifesting full cyclopia (class 5) (Fig. 2B), as well as lesser degrees of synopthalmia (class 2 and 3) (Supplemental Fig. S1A, Fig. 2H) (Marlow et al., 1998). We found that with the progression of the eye fusion phenotype, the shape of the cartilage elements, especially the ceratohyal, became more disrupted. However, this did not disturb the ability of the chondrocytes to stack (Fig. 2B, H Supplemental Fig S1A). This suggests that the craniofacial defect seen in the *wnt11* mutant fish is due primarily to the eye field separation defect displacing the cartilage elements. Because both *wnt5b* and *wnt11* are expressed in the zebrafish head and could possibly compensate for one another during craniofacial formation, we generated a *wnt5b*; *wnt11* double mutant to test if this would intensify the phenotype (Supplemental Fig. S1B). Phenotypic comparisons of the *wnt11* and *wnt5b; wnt11* mutants to the *wnt5b* mutant identified no observable difference, indicating a unique role of Wnt5b in control of chondrocyte stacking.

Three membrane-localized members of the core Wnt/PCP pathway, Vangl2, Scrib, and Gpc4, have zebrafish mutants with craniofacial defects. We investigated these mutants to see if the cartilage element defects were due to disruption of chondrocyte stacking. Zebrafish lacking a functional *vangl2* gene have previously been shown to have fused eyes due to the failure of the midline to bisect the eye field during early development (Marlow et al., 1998). This failure to divide the eye field not only disrupts the eyes, but also blocks the migratory path of premandibular neural crest cells, resulting in abnormal cartilage position (Fig. 2D). Despite this defect, many of the cartilage elements that are derived from other neural crest cell streams are not affected and the chondrocytes stack normally (Fig. 2D, J). The *scrib* mutant cartilage elements appear relatively normal compared to wild type siblings, with nicely defined stacked flat chondrocytes (Fig. 2E,K). However, s*crib* ceratohyals tended to bend in the mid-section of the element unlike their wild type siblings which had straight ceratohyals (Fig. 2A, E). In the *gpc4* mutant, Meckel's cartilage lost its bent arch shape (Fig. 2F) and both the ceratohyal and Meckel's cartilage were more compact, perpendicular to the anterior-posterior body axis, and composed of rounded cells in contrast to flattened chondrocytes found in wild type siblings and all but *wnt5b* mutants (Fig. 2F,L).

Overall, we hypothesized that the Wnt/PCP genes examined here can be classified into two craniofacial defect groups. The first group, *wnt11*, *scrib*, and *vangl2*, have cranial defects that affect cartilage element shape. The second group, *gpc4* and *wnt5b*, have distinct chondrocyte shape and stacking defects that underlie abnormal cartilage morphogenesis. To test this hypothesis we determined the ability of the chondrocytes of each of these mutants and their wild type siblings to produce the previously characterized thin and elongated chondrocyte shape of the ceratohyal (Kimmel et al., 1998). For each chondrocyte imaged, we measured the length and divided it by the width to get the length to width ratio (LWR). A perfectly round cell would have a ratio of 1, while a cell that is elongated would have a ratio greater than one. We first determined the mean LWR of 10 wild type stacked chondrocytes in the middle of 4 different ceratohyal elements, for a total of 40 cells measured. We found the wild type LWR mean to be 4.1 +/− 0.7. This same process was applied to each of the

characterized Wnt/PCP mutants (Table S1). As predicted; the *wnt11*, *scrib* and *vangl2* mutants had LWR values very similar to wild type whereas the *wnt5b* and *gpc4* mutants had ratios much closer to 1.6. This supports our hypothesis that these Wnt/PCP mutants can be grouped into two phenotypic classes. Based on these results, we will focus the rest of our study on *gpc4* and *wnt5b* as these two genes play a critical role in chondrocyte morphogenesis, which is the cause of their mutant cranial defects.

2.3 The neural crest migrates and is properly specified in gpc4 and wnt5b mutants

Vertebrate craniofacial cartilages arise from the cranial neural crest that migrates down in stereotypic streams to form the precursor pharyngeal arches (Crump et al., 2006; Knight and Schilling, 2006) which are separated by the pharyngeal endodermal pouches. To ascertain if the disorganized cartilage defect observed in *gpc4* and *wnt5b* mutants is due to problems with the specification and systematic migration and formation of the pharyngeal arches of the cranial neural crest, we assayed if these two early steps of cartilage formation were affected.

To determine if the neural crest is properly specified in *gpc4* and *wnt5b* mutants, we preformed whole mount *in situ* hybridization for pre-migratory neural crest markers *foxd3* (Odenthal and Nusslein-Volhard, 1998), *pax3* (Seo et al., 1998) and *sox10* (Dutton et al., 2001) on *gpc4* and *wnt5b* mutants and their wild type siblings at six somites (Fig. 3A–I). All three of these genes were expressed in *gpc4* and *wnt5b* mutants, outlining the broadened the neural plate, similar to the *dlx3* expression of *gpc4* mutants (Topczewski et al., 2001), indicating conversion and extension movement defects. The presence of pharyngeal arches within these mutants also appeared normal per the expression of the pharyngeal arch markers *dlx2* (Akimenko et al., 1994) at 28 hpf (Fig. 3J–L) and *dhand* (Thomas et al., 1998) at 32 hpf (Fig. 3M–O).

To examine if there is a cranial neural crest migration defect in *gpc4* or *wnt5b* mutants, we crossed the *Tg(fli1a:EGFP)*^{y1} reporter (Lawson and Weinstein, 2002) with *gpc4* and *wnt5b* which allowed us to observe the pharyngeal arch formation in wild type and mutant embryos. We stained fixed embryos with the Zn5 antibody to visualize the endodermal pouches as they are in direct contact with the arches. Mutant and wild type embryos at 36 hpf from both lines were examined for gross morphological defects in the developing pharynx (n=6 for each mutant and wild type sibling). We observed no difference between mutant and wild type siblings in the stereotypic migration and timing of the cranial neural crest cells into the pharyngeal arches (Fig. 3P–R). The anterio-posterior spacing of the pharyngeal arches was smaller, as a consequence of abnormal mutant embryo elongation, similar to the segmentation defects observed in the neural plate and somitic mesoderm domains during somitogenesis in both *gpc4* (Fig. 3Q) and *wnt5b* (Fig. 3R) mutants (Hammerschmidt et al., 1996; Topczewski et al., 2001). This defect is quite noticeable as the same size field of view was used for wild type and mutants reproducibly resulted in more pharyngeal arches visible in the mutants. We also did not find any dramatic differences in the endodermal pouches that separate the arches. These findings suggest that up to 36 hpf craniofacial cartilage development in both *wnt5b* and *gpc4* mutants is similar to wild type embryos. The only difference in the pharyngeal arch, all be it slight, is a result of

compaction of the embryo due to the early convergence and extension defect of these mutants.

2.4 Loss of wnt5b leads to a slight enhancement of the gpc4 mutant phenotype

While it is clear that a mutation in either *gpc4* or *wnt5b* leads to chondrocytes that are unable to elongate and form stacks within the cranial cartilage elements, the question arises of if these genes act together to achieve proper cartilage morphogenesis. In order to assess a potential genetic interaction between *gpc4* and *wnt5b* mutations in the control of craniofacial cartilage morphogenesis, the progeny of *gpc4* and *wnt5b* double heterozygotes were fixed and stained with Alcian blue at 5 dpf. For this analysis we used a missense allele *gpc4* ^{m818} that exhibits a weaker phenotype that can be enhanced by a genetic interaction (LeClair et al., 2009; Topczewski et al., 2001). The hyosymplectic, a cartilage element composed of three elements, the hyomandibula, the interhyal joint, and the symplectic (Fig. 4A), was dissected, flat mounted, and the length of the symplectic element was measured. The symplectic element was chosen as it is composed of a single row of stacked chondrocytes that is dramatically affected in *gpc4* and *wnt5b* mutants (LeClair et al., 2009). The length of the symplectic elements of the double homozygous mutant was not significantly different than the *gpc4*^{m818}; *wnt5b* $^{ta98/+}$ or *gpc4*$^{m818/+}$; *wnt5b* ^{ta98} symplectics, nor were the single heterozygous mutants significantly different from the double heterozygous mutants after the Bonferroni correction was applied (Fig. 4A). The double heterozygous mutants however were significantly different than wild type ($p = 0.0015$, Mann-Whtiney U(df) = 20) unlike their single heterozygote siblings (Fig. 4A). To demonstrate that the length of the symplectic element could be shorter than what is exhibited in the *gpc4*^{m818} mutant, the length of similarly staged symplectics of *gpc4*^{m818} mutants were compared with *gpc4*^{fr6} mutants, a nonsense allele that exhibits a more severe convergence and extension phenotype (Topczewski et al., 2001). As expected, the symplectic elements of the *gpc4*^{fr6} mutant were significantly shorter than the symplectic elements found in *gpc4*^{m818} embryos ($p = 0.0157$, Mann-Whitney U(df) = 22) (Fig. 4B).

2.5 The number of chondrocytes in craniofacial cartilages is unchanged in wnt5b and gpc4 mutants

When the *wnt5b* mutant was initially described, it was characterized as having many small cells (Piotrowski et al., 1996). Given that *wnt5b* promotes cell division in the long bone of mice (Yang et al., 2003) coupled with the initial observations of zebrafish *wnt5b* mutants, one might expect that the shorter craniofacial cartilage phenotype observed in the *wnt5b* mutants could be due to a change in cell number as compared to wild type. To determine if this was the case, 4 dpf *wnt5b*^{ta98} and *gpc4*^{fr6} embryos and their respective phenotypically wild type siblings were fixed and stained with DAPI and WGA (Figure 5A–C). The length, cell count, and volume of the ceratohyal and symplectic elements of the mutants and their respective wild type siblings were determined (Fig. 5E–H). Not surprisingly, there was a significant difference between the length of the mutant ceratohyal and symplectic elements and the elements of their wild type siblings ($p = <0.0001$, Mann-Whitney U(df) = 0) (Fig. 5E). There was no significant difference in the number of cells in the *wnt5b*^{ta98} and *gpc4* ^{fr6} mutant ceratohyal when compared to their wild type siblings (Fig. 5F). Interestingly, there was a signifignant difference between the *wnt5b*^{ta98} and their wild type sibling symplectic

elements (p = 0.0022, Mann-Whitney U (df) = 4.5) but not the between the *gpc* ^{fr6} symplectics and their wild type siblings (Fig. 5F). While there was not a difference between the average volume of the ceratohyal in the *wnt5b*^{ta98} mutants and the wild type siblings, a significant difference did exist between *gpc4*^{fr6} ceratohyal and symplectic elements and their wild type siblings (p = <0.0001, Mann-Whitney U(df) = 0) (Fig. 5G).

The difference in the volume of the ceratohyal elements in *gpc4*^{fr6} mutants but not the *wnt5b*^{ta98} mutants prompted us to ask if the cells of *gpc4* ^{fr6} mutants are smaller. We measured the volume of 20 cells at the proximal end and in the center of three different ceratohyal elements from *gpc4* ^{fr6} and wild type siblings. We found that there was a significant difference between the volume of both the center and proximal end between wild type and mutant cartilage elements (center p = <0.0001, Mann-Whitney U(df) = 854; proximal p = 0.0004, Mann-Whitney U(df) = 1131) (Fig. 5H). Interestingly, the volume of the cells at the center of the *gpc4* ^{fr6} mutant ceratohyals is not significantly different from the volume of the cells at the proximal end of this element in the wild type siblings.

2.6 In craniofacial cartilage Gpc4 acts cell autonomously

To help determine the mode of action of Gpc4 and Wnt5b within craniofacial cartilage, we set out to identify if these proteins acted cell autonomously or cell non-autonomously within cartilage development. When *wnt5b* mutant cells were transplanted to wild type embryos, there was no effect on the morphology of the cartilage (Table 1). Similarly, if a small number of wild type cells were transplanted next to a cartilage or within a *wnt5b* mutant element, no effect was seen. In contrast, a large number of wild type cells transplanted to and around *wnt5b* mutant chondrocytes appeared to suppress the mutant phenotype, and restore the elongated and stacked chondrocyte organization (Fig. 6A–L), suggesting that the *wnt5b* mutant cells act non-autonomously. To quantify these results the LWR of the transplanted cells was determined in three regions of the ceratohyal (Region A, proximal; Region B, center; and Region C, distal). The average length to width ratios of the transplanted cells from each region was then compared to the neighboring chondrocytes (Table 1). When the length to width ratios of the transplanted wild type chondrocytes were compared to their neighboring *wnt5b* mutant neighbors they were not significantly different than the neighboring cells (Table 1).

When wild type cells were transplanted into the chondrocytes of *gpc4* mutants then the cells would elongate as demonstrated in the Meckel's cartilage transplant shown in Fig. 6M–P. When wild type cells were transplanted to *gpc4* hosts in region B of the certatohyal and the length to width ratio was compared to the control the results were significant (p = 0.0004, Mann Whitney U(df) = 2) (Table 1). However, if wild type cells were transplanted into the most proximal and distal regions of the *gpc4* mutant ceratoyhal (Regions A and C) the cells retain their mutant morphology as the length to width ratio of the transplanted cells was not significant when compared to their mutant neighboring cells (Table 1).

When *gpc4* mutant cells were transplanted into wild type cartilage, the cells would respond in an autonomous fashion and develop the round phenotype characteristic of *gpc4* mutant chondrocytes (Fig. 6 Q–T). When quantified, the length to width ratios of transplanted chondrocytes in regions A, B, and C of the ceratohyal are significantly different from their

neighbors (Region A p = <0.0001, Mann -Whitney U(df) = 208; Region B p <0.0001, Mann -Whitney U(df) = 32; Region C p = 0.0002, Mann-Whitney U(df) = 75) (Table 1).

3. Discussion

3.1 Proper chondrocyte elongation and stacking depends on Wnt5b and Gpc4 activity

While the genes for the core members of the PCP pathway, *wnt11* and *vangl2* are both expressed in pharyngeal arches (Fig. 1C–D', K–L'), the misshapen cartilage elements found in these mutants are capable of forming elongated and stacked chondrocytes (Fig. 2J, L, M). The *wnt11* and *vangl2* mutations seem to affect craniofacial development in an indirect way as a result of synopthalmia leading to improper head morphology. The lack of a cartilage stacking phenotype cannot be due to redundancy. This is evident in the fact that as the severity of the synophthalmia within these mutants decreases so does the severity of the craniofacial cartilage defects. While we cannot be certain that the removal of maternal and zygotic contributions or the creation of stronger loss of function *vangl2* or *wnt11* mutants would not create stacking defects, *gpc4* and *wnt5b* mutants are both unable to create stacked and elongated craniofacial chondrocytes and therefore disrupt cartilage formation directly (Fig. 2H, K).

3.2 Loss of gpc4 leads to smaller chondrocytes and a decreased cartilage element volume

Although Wnt5b promotes cell division in long bones of mice (Yang et al., 2003), in zebrafish *wnt5b* mutants, the number of cells of the ceratohyal cartilage remained the same compared to their wild type siblings (Fig. 5F). As our studies focused on 4 dpf, we cannot exclude the possibility that defects in cell proliferation may occur in later stages of development. Similarly, the loss of *wnt5b* does not affect the volume of the ceratohyal elements (Fig. 5G). The loss of *gpc4* does affect the volume of the ceratohyal and symplectic elements, as they are both significantly smaller than their wild type siblings (Fig. 5G). The smaller element volume suggests that either the chondrocyte volume itself is smaller or there is less extracellular matrix (ECM) within the *gpc4* mutant. While we found that the volume of mutant chondrocytes is smaller than the wild type, the fold of the change (reduction of 22% proximal chondrocytes and 26% of chondrocytes in the center) cannot completely account for the 37% decrease of total ceratohyal volume (Fig. 5G and H). This observation suggests the reduced production of ECM and indicates delayed or inhibited differentiation. Interestingly, cartilage ECM ultra structure of *gpc4* mutants was reported to be normal (Wiweger et al., 2011). Despite the reduction of the mutant chondrocyte volume, the trend to increase the volume of the chondrocytes between the proximal and center part of the ceratohyal is maintained (1.34 WT and 1.29 for *gpc4*). This observation indicates that Gpc4 is not crucial for proximal central patterning of the chondrocytes. Importantly, endochondrial ossification is not inhibited in *gpc4* mutants (LeClair et al., 2009), indicating a specific requirement for Glypican 4 in chondrocyte stacking.

3.3 The cell autonomy of gpc4 and wnt5b

Despite the fact that we did not see an enhancement of the *gpc4* phenotype in the *gpc4; wnt5b* double mutants in craniofacial cartilage, we expect that chondrocytes would respond to these genes cell autonomously and cell non-autonomously given that they act as a co-

receptor and a ligand respectively. Previous work by Li and Dudley (2009) demonstrated that the downstream targets of the Wnt/PCP pathway Fzd7 and Dsh act cell-autonomously in the long bone of chick embryos. While *gpc4* and *wnt5b* share overlapping gene expression patterns at 55 hpf (Fig 1N and O), our transplantation experiments compliment Li and Dudley's work as *gpc4* acts cell autonomously within the craniofacial cartilage at 5 dpf (Figure 6M–T and Table 1) and therefore act in the manner appropriate to the molecule's known function. The results of the *wnt5b* transplantations suggest that the transplanted wild type cells did not produce enough Wnt5b to fully rescue the mutant *wnt5b* host elements (Figure 6A–L and Table 1). This result is not surprising as Wnt5b is a morphogen and suggests that the chondrocytes only elongate in response to high levels of the Wnt5b protein.

3.4 The role of gpc4 and wnt5b in craniofacial cartilage morphogenesis

We demonstrated that *gpc4* and *wnt5b* do not behave like the other core Wnt/PCP molecules within zebrafish craniofacial development however, the mechanism in which they influence chondrocyte shape is still unclear. Clearly, *gpc4* and *wnt5b* act as part of the Wnt/PCP pathway in convergence and extension of the main body axes (Kilian et al., 2003; Topczewski et al., 2001) but within chondrocyte morphogenesis they appear to act independently of *vangl2*, one of the pathway's core molecules. Genetic interaction studies show that the addition of one copy of *wnt5b* enhances the phenotype of *gpc4* heterozygotes, but an enhancement is not seen when comparing double mutants (Fig. 3A). These results suggest a slight interaction; however null mutants would be needed to establish any epistatic relationship. Gpc4 may participate in other developmental processes, but without Wnt5b, properly stacked chondrocytes cannot form suggesting that all of Wnt5b's activity in cartilage morhphogenesis goes through Gpc4. These results lead to the question of how these genes affect the ultimate shape and volume of the cartilage elements outside of the other core Wnt/PCP pathway molecules such as *vangl2*.

Studies by Bradley and Drissi (2011) may shed some light into the role of *wnt5b* and *gpc4* in cartilage morphogenesis as experiments demonstrate that in limb bud micro mass cultures, *wnt5b* acts to regulate osteochondroprogenitor cell migration through JNK and decreases cell adhesion by regulating the stability of cadherin receptors. This loss of adhesion is echoed by the loss of membrane associated β-catenin and an increase in nuclear β-catenin. Although done in culture, this demonstrates the possibility that *wnt5b* may act to regulate JNK and cadherin within zebrafish craniofacial cartilage morphogenesis. Furthermore, recent evidence by Romereim et al. (2014) demonstrates that chondrocyte stacking in the presphenoidal synchondrosis of mice depends on p-catenin and cadherin adhesion to properly orient the chondrocytes. Their data suggests that Wnt/PCP signaling may control chondrocyte stacking once the cell has divided. Chondrocytes of craniofacial cartilage elements in zebrafish embryo form stacks after mesenchymal condensation suggesting mechanisms of cell orientation independent of cell division.

Another gene that could be involved in zebrafish craniofacial cartilage morphogenesis is *ror2*. This gene along with *Wnt5a* has been shown to genetically and physically interact with *Vangl2* within mice (Gao et al., 2011; Topczewski et al., 2011; Wang et al., 2011). While the loss of these genes leads to long bone and digit phenotypes, they are also expressed in

craniofacial cartilage suggesting they may also play a role in its morphogenesis. If the loss of *Vangl2* and *Wnt5a* leads to long bone and digit phenotypes in mice, why does the phenotype associated with the loss of *vangl2* appear to be an effect of the cyclopia found in the mutant and not due to a stacking or intercalation defect of the chondrocytes? Most of the studies done with these two genes involve cells that are in direct contact with each other such as the *Drosophila* wing or larval epidermis (Simons and Mlodzik, 2008). Chondrocytes, with the exception of dividing cells, cannot depend on direct cell-cell contact due to the large amount of extracellular matrix that separates them and forms the cartilage element. In chicks, the overexpression of *Vangl2* leads to disorganized chondrocytes within wing cartilage (Li and Dudley, 2009) likely due to disruption of the Wnt-PCP signaling. We observed largely normal morphology of chondrocytes in *vangl2* mutants (Fig. 2J), despite *vangl2* expression in the branchial arches at the time of cartilage condensation (Fig. 1C–D', M). We hypothesize that in the absence of direct contact, chondrocytes depend on elements of the Wnt/PCP pathway that receive long distance signaling, including Wnt5b and Gpc4, and do not utilize *vangl2* in order to achieve proper cell orientation, intercalation and stacking.

Mutations in genes that are not directly involved with signaling but are involved with the cellular processing of signaling molecules may also lead to stacking and intercalation defects in zebrafish cartilage elements. Two of these genes are *exostosin* (*ext1* and *2*). The loss of *ext 1/2* leads to a phenotype that is reminiscent of *wnt5b* and *gpc4* mutants as they too have smaller cartilage elements with rounded chondrocytes (Clement et al., 2008). As these genes are necessary for the proper posttranslational modification of proteoglycans within the Golgi apparatus, the cartilage phenotype that results from their loss highlights the importance of glypicans and their heparan sulfate side chains within this developmental process.

3.4 Conclusions

The experiments put forth here demonstrate that chondrocyte stacking defects observed in *wnt5b* and *gpc4* mutants are most likely due to defects in intercalation. This process is independent of *vangl2*, *wnt11*, and *scrib* indirect head morphology defects. This independent role of Gpc4 and Wnt5b from the core Wnt/PCP molecules is not similar to what occurs in zebrafish convergence and extension (Heisenberg et al., 2000; Jessen et al., 2002; Park and Moon, 2002; Rauch et al., 1997; Topczewski et al., 2001; Wada et al., 2005). During gastrulation, the moving cells are very close together, providing an opportunity for cell-cell interactions. This is not the case in zebrafish cartilage morphogenesis as the extracellular matrix is laid down between the chondrocytes. While Gpc4 and Wnt5b appear to act together to control cartilage stacking and morphogenesis, there are likely other, yet not unidentified, player(s) that also act(s) through Gpc4.

4. Experimental Procedures

4.1 Zebrafish maintenance, embryo production and staging

AB [ZFIN ID:ZDB-GENO-960809-7], *gpc4*^{m818} [ZFIN ID:ZDB-GENO-011120-5], *gpc4*^{fr6} [ZFIN ID:ZDB-GENO-120430-1], *wnt5b*^{ta98} [ZFIN ID:ZDB-GENO-980202-1367],

wnt11^{tz216} [ZFIN ID:ZDB-GENO-980202-1408], and *Tg(fli1a:EGFP)*^{y1} [ZDB-GENO-011017-4] zebrafish lines were maintained as described in Topczewski et al. (2001). Embryos were collected from natural spawning and staged according to morphology described in Kimmel et al. (1995). The fish protocols and care in this paper were approved by the IACUC of Stanley Manne Children's Research Institute (Chicago, IL), an AALAC-accredited facility.

4.2 In situ hybridization

Anti-sense RNA probes were synthesized using the following cDNA clones: *vangl1* [GenBank:NM_205750, ZFIN ID:ZBD-GENE-040621-2], *vangl2* [GenBank:NM_153674, ZFIN ID:ZBD-GENE-020507-3], *wnt5b* [GenBank:NM_130937, ZFIN ID:ZBD-GENE-980526-87], *gpc4* [GenBank:NM_131860, ZFIN ID:ZBD-GENE-011119-1], *foxd3* [GenBank:NM_131290, ZFIN ID:ZBD-GENE-980526-143], *pax3a* [GenBank:NM_131277, ZFIN ID:ZBD-GENE-980526-52], *sox10* [GenBank:NM_131875, ZFIN ID:ZBD-GENE-011207-1], *dlx2a* [GenBank:NM_131311, ZFIN ID:ZBD-GENE-980526-212], *wnt11* [GenBank:NM_001144804, ZFIN ID:ZBD-GENE-990603-12] and *dhand* GenBank:NM_131626, ZFIN ID:ZBD-GENE-000511-1]. Whole mount *in situ* hybridization was performed as described in Topczewski et al. (2001) and at least 40 embryos were analyzed for each gene.

4.3 Cranial neural crest migration imaging

The *Tg(fli1a:EGFP)*^{y1} zebrafish line, a kind gift from Dr. Nathan Lawson, was crossed with *wnt5b*$^{ta98/+}$ and *gpc4*$^{r6/+}$ allelic lines to generate heterozygous mutants that carried the *fli1a:EGFP* transgene. The offspring of these out-crosses were then in-crossed to siblings to generate *Tg(fli1a:EGFP)*^{y1}*; wnt5b*^{ta98} and *Tg(fli1a:EGFP)*^{y1}*; gpc4*^{fr6} mutant embryos. From 24 hpf, embryos were exposed to 0.003% 1-phenyl-2-thiourea to prevent pigment formation and fixed overnight at 4°C in 4% paraformaldehyde (3PFA) at 36 hpf. Embryos were washed and then stained with an anti-Zn5 mouse monoclonal antibody [ZDB-ATB-081002-19] from the Zebrafish International Resource Center (ZIRC), which recognizes the Alcama protein. At 36 hpf, the Zn5 antibody marks the pharyngeal endodermal pouches along with other tissues. The fixed specimens were whole mounted and imaged using the Zeiss LSM 510 confocal microscope. Z-stacks were taken of at least six different embryos.

4.4 Cartilage imaging

Embryos were fixed and stained with Wheat Germ Agglutinin (WGA) (Invitrogen) and DAPI (Sigma-Aldrich) as described in Dale and Topczewski (2011). Z-stack images of the embryos were taken using either a Zeiss LSM 510 or LSM 700 laser confocal microscope.

4.5 Stacked chondrocyte measurements

Wild type and PCP mutant 4 dpf embryos were fixed and mounted as described in *Cartilage imaging* above. Representative ceratohyals for each mutant and wild type were chosen and their Z-stack images were analyzed to determine chondrocytes ability to elongate and stack as previously characterized (Kimmel et al., 1998). Using the ZEN Blue Edition software

(Zeiss), we determined the middle of the ceratohyal where in wild type the element is composed of elongated and stacked chondrocytes and then measured the length and width of 10 representative cells around the middle of the cartilage element. This was done for 4 ceratohyal elements from at least 2 different embryos, providing us with n=40 chondrocytes measured for each category. Measurements were inputted into the statistics program Prism 6 (GraphPad) to determine ratio of length to width for each chondrocyte and plotted with their cohort to determine the average and standard deviation for each mutant's length to width ratio along with the D'Agostino and Pearson omnibus normality test to determine if the data sets were normalized and P-values were determined.

4.6 Cartilage element length, volume, and cell count

To determine if there is a genetic interaction between *wnt5b* and *gpc4*, Alcian blue stainings of 5 dpf progeny of *wnt5b*$^{ta98/+}$; *gpc4*$^{m818/+}$ mutant fish, as well as *gpc4*^{m818}, *gpc4*^{fr6} and their wild type siblings were done as described in Walker and Kimmel (2007). The Alcian blue stained embryos were imaged and the symplectic elements were dissected, the embryos genotyped, and imaged and measured using an AxioPlan 2 microscope and AxioVision (4.8.1) software (Zeiss). To determine the volume, chondrocyte count and length of the ceratohyals and symplectics elements, wild type (AB), *wnt5b*^{ta98} and *gpc4*^{fr6} 4 dpf embryos were fixed, stained with WGA and DAPI and imaged as above. The lengths of the ceratohyal and symplectic elements were taken using ZEN 2009 Light Edition software (Zeiss). The volume and cell count of the ceratohyal and symplectic elements were determined by analyzing confocal z-stacks with Amira 5.4.1 3D imaging software (Visage Imaging). All statistics were done using Mann-Whitney U tests using Prism 6 (Graph Pad).

4.7 Cell transplantation

Donor embryos were injected with Rhodamine/biotinylated dextran (total dextran 5%, 10,000 MW) (Molecular Probes) in 0.2M KCl at the one to two cell stage. Donor and recipient embryos were raised at 28°C until they reached dome stage at which time the cells were transplanted from the donor to the recipient embryos at the blastula margin using a Cell Tram Vario (Eppendorf) in 1X Niu-Twitty buffer with HEPES (Niu and Twitty, 1953). The transplantations continued until both sets of embryos reached the shield stage. Following transplantation, the embryos were allowed to recover at 28°C overnight in 0.3X Niu-Twitty Buffer with HEPES and 5% Pen-Strep. At 1 dpf the embryos were screened for transplanted cells in the pharangeal arches and these embryos were allowed to grow to 5 dpf in egg water at 28°C stage. The successfully transplanted embryos were then fixed at 5 dpf using 4% PFA overnight, washed extensively in 1X PBS + 0.01% Trixton (PBST), treated with 0.05% trypsin for 25 minutes at room temperature, washed extensively with PBST, stained with WGA and DAPI per the protocol above and stained using Steptavadin (Alexa Fluor 488, Invitrogen) at 1:100 in PBST at room temperature for 1 hour. The embryos were then imaged as described above. The n values of embryos analyzed with transplants into craniofacial cartilage are as follows: 31 wild type donor to wild type hosts, 7 wild type donor to *gpc4* mutant hosts, 1 *wnt5b* mutant donor to wild type host, 6 wild type donor to *wnt5b* mutant hosts, 31 wild type donor to wild type host, and 16 *gpc4* donor to wild type hosts.

To quantify the transplantation results we focused on those embryos with transplantations to the ceratohyal. Using the confocal z-stack and ZEN 2012 Light Edition software (Zeiss), the length of ceratohyals were obtained and the elements were divided into 3 equal sections (Region A, proximal; Region B, center; Region C, distal). The length and width of the transplanted cells within the chondrocytes of these 3 regions was then obtained. All statistics were done using Mann-Whitney U tests using Prism 6 (Graph Pad).

4.9 Cyrosections

The cyrosections were performed per Sisson and Topczewski (2009).

Supplementary Material

Refer to Web version on PubMed Central for supplementary material.

Acknowledgements

We would like to thank Mr. Marco Rhein and Mr. Jonathan Sager for data collection assistance, Dr. Elizabeth LeClair and Dr. Chester Ismay for statistical analysis advice, Ms. Rebecca Anderson for providing critical comments on this manuscript, Dr. Jason Jesson for providing the *vangl1* and *vangl2* probes, and Dr. Nathan Lawson for providing the *Tg(fli1a:EGFP)*^{y1} zebrafish line. This work was supported by the National Institutes of Health - NIDCR Grants: R01DE016678 to (JT), F32DE019058 (BES), and F32DE019986 (RMD).

References

Akimenko MA, Ekker M, Wegner J, Lin W, Westerfield M. Combinatorial expression of three zebrafish genes related to distal-less: part of a homeobox gene code for the head. J Neurosci. 1994; 14:3475–3486. [PubMed: 7911517]

Bradley EW, Drissi MH. Wnt5b regulates mesenchymal cell aggregation and chondrocyte differentiation through the planar cell polarity pathway. J Cell Physiol. 2011; 226:1683–1693. [PubMed: 21413026]

Carmona-Fontaine C, Matthews HK, Kuriyama S, Moreno M, Dunn GA, Parsons M, Stern CD, Mayor R. Contact inhibition of locomotion in vivo controls neural crest directional migration. Nature. 2008; 456:957–961. [PubMed: 19078960]

Clay MR, Halloran MC. Regulation of cell adhesions and motility during initiation of neural crest migration. Curr Opin Neurobiol. 2011; 21:17–22. [PubMed: 20970990]

Clement A, Wiweger M, von der Hardt S, Rusch MA, Selleck SB, Chien CB, Roehl HH. Regulation of zebrafish skeletogenesis by ext2/dackel and papst1/pinscher. PLoS Genet. 2008; 4:e1000136. [PubMed: 18654627]

Crump JG, Swartz ME, Eberhart JK, Kimmel CB. Moz-dependent Hox expression controls segment-specific fate maps of skeletal precursors in the face. Development. 2006; 133:2661–2669. [PubMed: 16774997]

Cubbage CC, Mabee PM. Development of the cranium and paired fins in the zebrafish Danio rerio (Ostariophysi cyprindae). Journal of Morphology. 1996; 229:121–160.

Dale RM, Sisson BE, Topczewski J. The emerging role of Wnt/PCP signaling in organ formation. Zebrafish. 2009; 6:9–14. [PubMed: 19250029]

Dale RM, Topczewski J. Identification of an evolutionarily conserved regulatory element of the zebrafish col2a1a gene. Dev Biol. 2011; 357:518–531. [PubMed: 21723274]

De Calisto J, Araya C, Marchant L, Riaz CF, Mayor R. Essential role of non-canonical Wnt signalling in neural crest migration. Development. 2005; 132:2587–2597. [PubMed: 15857909]

Dutton KA, Pauliny A, Lopes SS, Elworthy S, Carney TJ, Rauch J, Geisler R, Haffter P, Kelsh RN. Zebrafish colourless encodes sox10 and specifies non-ectomesenchymal neural crest fates. Development. 2001; 128:4113–4125. [PubMed: 11684650]

Gao B, Song H, Bishop K, Elliot G, Garrett L, English MA, Andre P, Robinson J, Sood R, Minami Y, Economides AN, Yang Y. Wnt signaling gradients establish planar cell polarity by inducing Vangl2 phosphorylation through Ror2. Dev Cell. 2011; 20:163–176. [PubMed: 21316585]

Glickman NS, Kimmel CB, Jones MA, Adams RJ. Shaping the zebrafish notochord. Development. 2003; 130:873–887. [PubMed: 12538515]

Gubb D, Garcia-Bellido A. A genetic analysis of the determination of cuticular polarity during development in Drosophila melanogaster. J Embryol Exp Morphol. 1982; 68:37–57. [PubMed: 6809878]

Hammerschmidt M, Pelegri F, Mullins MC, Kane DA, Brand M, van Eeden FJ, Furutani-Seiki M, Granato M, Haffter P, Heisenberg CP, Jiang YJ, Kelsh RN, Odenthal J, Warga RM, Nusslein-Volhard C. Mutations affecting morphogenesis during gastrulation and tail formation in the zebrafish, Danio rerio. Development. 1996; 123:143–151. [PubMed: 9007236]

Heisenberg CP, Brand M, Jiang YJ, Warga RM, Beuchle D, van Eeden FJ, Furutani-Seiki M, Granato M, Haffter P, Hammerschmidt M, Kane DA, Kelsh RN, Mullins MC, Odenthal J, Nusslein-Volhard C. Genes involved in forebrain development in the zebrafish, Danio rerio. Development. 1996; 123:191–203. [PubMed: 9007240]

Heisenberg CP, Tada M, Rauch GJ, Saude L, Concha ML, Geisler R, Stemple DL, Smith JC, Wilson SW. Silberblick/Wnt11 mediates convergent extension movements during zebrafish gastrulation. Nature. 2000; 405:76–81. [PubMed: 10811221]

Jessen JR, Solnica-Krezel L. Identification and developmental expression pattern of van gogh-like 1, a second zebrafish strabismus homologue. Gene Expr Patterns. 2004; 4:339–344. [PubMed: 15053985]

Jessen JR, Topczewski J, Bingham S, Sepich DS, Marlow F, Chandrasekhar A, Solnica-Krezel L. Zebrafish trilobite identifies new roles for Strabismus in gastrulation and neuronal movements. Nat Cell Biol. 2002; 4:610–615. [PubMed: 12105418]

Kilian B, Mansukoski H, Barbosa FC, Ulrich F, Tada M, Heisenberg CP. The role of Ppt/Wnt5 in regulating cell shape and movement during zebrafish gastrulation. Mech Dev. 2003; 120:467–476. [PubMed: 12676324]

Kimmel CB, Ballard WW, Kimmel SR, Ullmann B, Schilling TF. Stages of embryonic development of the zebrafish. Dev Dyn. 1995; 203:253–310. [PubMed: 8589427]

Kimmel CB, Miller CT, Kruze G, Ullmann B, BreMiller RA, Larison KD, Snyder HC. The shaping of pharyngeal cartilages during early development of the zebrafish. Dev Biol. 1998; 203:245–263. [PubMed: 9808777]

Knight RD, Schilling TF. Cranial neural crest and development of the head skeleton. Adv Exp Med Biol. 2006; 589:120–133. [PubMed: 17076278]

Lawson ND, Weinstein BM. In vivo imaging of embryonic vascular development using transgenic zebrafish. Dev Biol. 2002; 248:307–318. [PubMed: 12167406]

LeClair EE, Mui SR, Huang A, Topczewska JM, Topczewski J. Craniofacial skeletal defects of adult zebrafish Glypican 4 (knypek) mutants. Dev Dyn. 2009; 238:2550–2563. [PubMed: 19777561]

Li Y, Dudley AT. Noncanonical frizzled signaling regulates cell polarity of growth plate chondrocytes. Development. 2009; 136:1083–1092. [PubMed: 19224985]

Lin F, Sepich DS, Chen S, Topczewski J, Yin C, Solnica-Krezel L, Hamm H. Essential roles of G{alpha}12/13 signaling in distinct cell behaviors driving zebrafish convergence and extension gastrulation movements. J Cell Biol. 2005; 169:777–787. [PubMed: 15928205]

Lopez-Schier H, Hudspeth AJ. A two-step mechanism underlies the planar polarization of regenerating sensory hair cells. Proc Natl Acad Sci U S A. 2006; 103:18615–18620. [PubMed: 17124170]

Lopez-Schier H, Starr CJ, Kappler JA, Kollmar R, Hudspeth AJ. Directional cell migration establishes the axes of planar polarity in the posterior lateral-line organ of the zebrafish. Dev Cell. 2004; 7:401–412. [PubMed: 15363414]

Marlow F, Zwartkruis F, Malicki J, Neuhauss SC, Abbas L, Weaver M, Driever W, Solnica-Krezel L. Functional interactions of genes mediating convergent extension, knypek and trilobite, during the partitioning of the eye primordium in zebrafish. Dev Biol. 1998; 203:382–399. [PubMed: 9808788]

Matthews HK, Marchant L, Carmona-Fontaine C, Kuriyama S, Larrain J, Holt MR, Parsons M, Mayor R. Directional migration of neural crest cells in vivo is regulated by Syndecan-4/Rac1 and non-canonical Wnt signaling/RhoA. Development. 2008; 135:1771–1780. [PubMed: 18403410]

Niu MC, Twitty VC. The Differentiation of Gastrula Ectoderm in Medium Conditioned by Axial Mesoderm. Proc Natl Acad Sci U S A. 1953; 39:985–989. [PubMed: 16589364]

Odenthal J, Nusslein-Volhard C. fork head domain genes in zebrafish. Dev Genes Evol. 1998; 208:245–258. [PubMed: 9683740]

Parichy DM, Elizondo MR, Mills MG, Gordon TN, Engeszer RE. Normal table of postembryonic zebrafish development: staging by externally visible anatomy of the living fish. Dev Dyn. 2009; 238:2975–3015. [PubMed: 19891001]

Park M, Moon RT. The planar cell-polarity gene stbm regulates cell behaviour and cell fate in vertebrate embryos. Nat Cell Biol. 2002; 4:20–25. [PubMed: 11780127]

Piotrowski T, Schilling TF, Brand M, Jiang YJ, Heisenberg CP, Beuchle D, Grandel H, van Eeden FJ, Furutani-Seiki M, Granato M, Haffter P, Hammerschmidt M, Kane DA, Kelsh RN, Mullins MC, Odenthal J, Warga RM, Nusslein-Volhard C. Jaw and branchial arch mutants in zebrafish II: anterior arches and cartilage differentiation. Development. 1996; 123:345–356. [PubMed: 9007254]

Rauch GJ, Hammerschmidt M, Blader P, Schauerte HE, Strahle U, Ingham PW, McMahon AP, Haffter P. Wnt5 is required for tail formation in the zebrafish embryo. Cold Spring Harb Symp Quant Biol. 1997; 62:227–234. [PubMed: 9598355]

Romereim SM, Conoan NH, Chen B, Dudley AT. A dynamic cell adhesion surface regulates tissue architecture in growth plate cartilage. Development. 2014; 141:2085–2095. [PubMed: 24764078]

Schilling TF, Piotrowski T, Grandel H, Brand M, Heisenberg CP, Jiang YJ, Beuchle D, Hammerschmidt M, Kane DA, Mullins MC, van Eeden FJ, Kelsh RN, Furutani-Seiki M, Granato M, Haffter P, Odenthal J, Warga RM, Trowe T, Nusslein-Volhard C. Jaw and branchial arch mutants in zebrafish I: branchial arches. Development. 1996; 123:329–344. [PubMed: 9007253]

Seo HC, Saetre BO, Havik B, Ellingsen S, Fjose A. The zebrafish Pax3 and Pax7 homologues are highly conserved, encode multiple isoforms and show dynamic segment-like expression in the developing brain. Mech Dev. 1998; 70:49–63. [PubMed: 9510024]

Simons M, Mlodzik M. Planar cell polarity signaling: from fly development to human disease. Annu Rev Genet. 2008; 42:517–540. [PubMed: 18710302]

Sisson BE, Topczewski J. Expression of five frizzleds during zebrafish craniofacial development. Gene Expr Patterns. 2009; 9:520–527. [PubMed: 19595791]

Solnica-Krezel L, Stemple DL, Mountcastle-Shah E, Rangini Z, Neuhauss SC, Malicki J, Schier AF, Stainier DY, Zwartkruis F, Abdelilah S, Driever W. Mutations affecting cell fates and cellular rearrangements during gastrulation in zebrafish. Development. 1996; 123:67–80. [PubMed: 9007230]

Thomas T, Kurihara H, Yamagishi H, Kurihara Y, Yazaki Y, Olson EN, Srivastava D. A signaling cascade involving endothelin-1, dHAND and msx1 regulates development of neural-crest-derived branchial arch mesenchyme. Development. 1998; 125:3005–3014. [PubMed: 9671575]

Topczewski J, Dale RM, Sisson BE. Planar cell polarity signaling in craniofacial development. Organogenesis. 2011; 7:255–259. [PubMed: 22134372]

Topczewski J, Sepich DS, Myers DC, Walker C, Amores A, Lele Z, Hammerschmidt M, Postlethwait J, Solnica-Krezel L. The zebrafish glypican knypek controls cell polarity during gastrulation movements of convergent extension. Dev Cell. 2001; 1:251–264. [PubMed: 11702784]

Wada H, Iwasaki M, Sato T, Masai I, Nishiwaki Y, Tanaka H, Sato A, Nojima Y, Okamoto H. Dual roles of zygotic and maternal Scribble1 in neural migration and convergent extension movements in zebrafish embryos. Development. 2005; 132:2273–2285. [PubMed: 15829519]

Wada H, Okamoto H. Roles of noncanonical Wnt/PCP pathway genes in neuronal migration and neurulation in zebrafish. Zebrafish. 2009; 6:3–8. [PubMed: 19250033]

Walker MB, Kimmel CB. A two-color acid-free cartilage and bone stain for zebrafish larvae. Biotech Histochem. 2007; 82:23–28. [PubMed: 17510811]

Wang B, Sinha T, Jiao K, Serra R, Wang J. Disruption of PCP signaling causes limb morphogenesis and skeletal defects and may underlie Robinow syndrome and brachydactyly type B. Hum Mol Genet. 2011; 20:271–285. [PubMed: 20962035]

Wiweger MI, Avramut CM, de Andrea CE, Prins FA, Koster AJ, Ravelli RB, Hogendoorn PC. Cartilage ultrastructure in proteoglycan-deficient zebrafish mutants brings to light new candidate genes for human skeletal disorders. J Pathol. 2011; 223:531–542. [PubMed: 21294126]

Yang Y, Topol L, Lee H, Wu J. Wnt5a and Wnt5b exhibit distinct activities in coordinating chondrocyte proliferation and differentiation. Development. 2003; 130:1003–1015. [PubMed: 12538525]

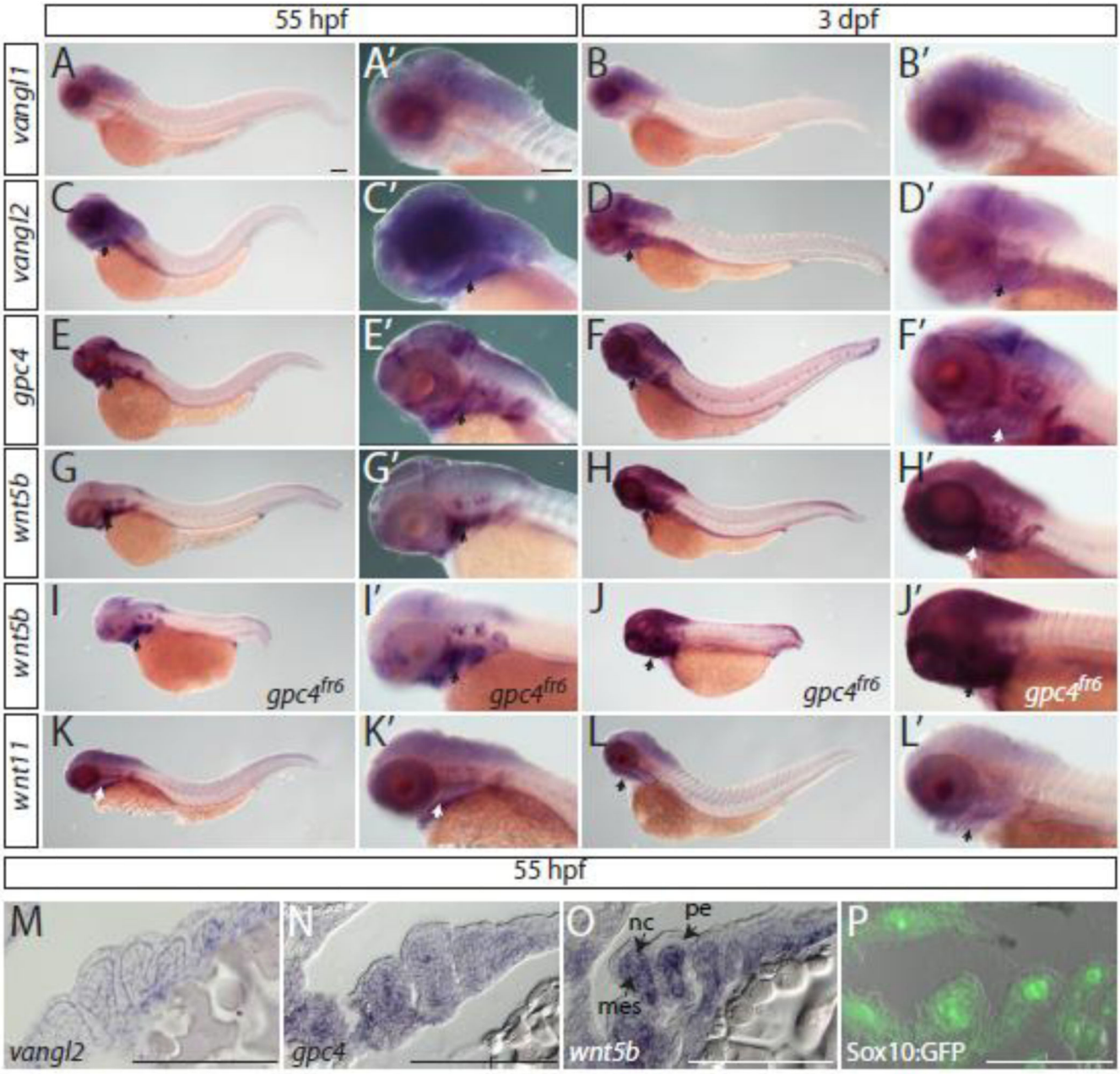

Fig. 1. Expression of Wnt/PCP molecules in the zebrafish head of 55 hours hpf and 3 dpf embryos

(A–H', K–L') *In situ* hybridizations of whole mount wild type embryos. (I–J') *wnt5b* expression in *gpc4*^{fr6} mutant embryos. (A–L') Arrows indicate staining in the pharyngeal arches. (M–P) Sections of whole mount *in situ* hybridizations. (M) *vangl2* is expressed in the mes and nc. (N) *gpc4* is expressed in the pe, mes and the nc. (O) *wnt5b* is expressed in the mes and nc. (P) Sox10:GFP expression in the mes and in the nc. Abbreviations: mes = mesoderm, nc = neural crest, pe = pharyngeal endoderm. Scale bar = 100 μm.

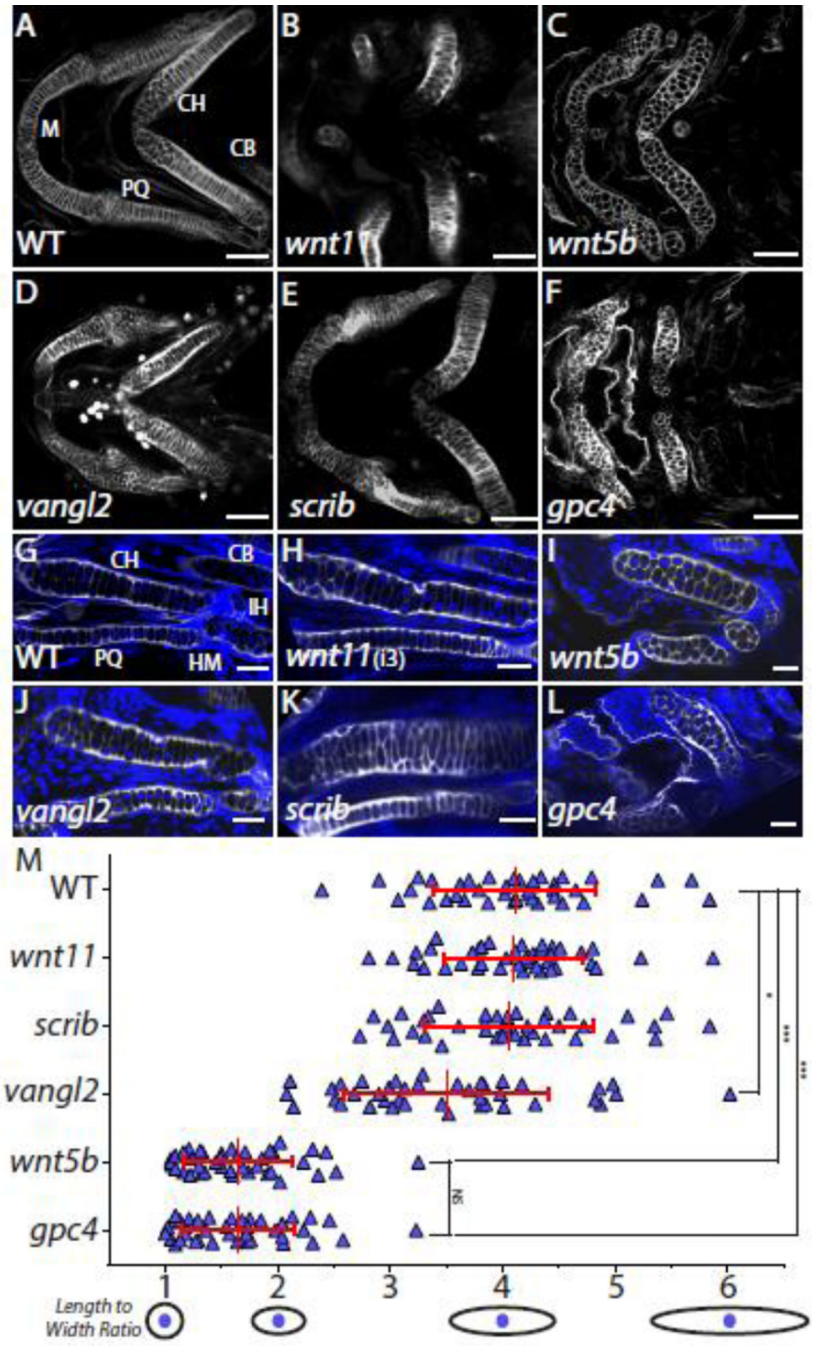

Fig. 2. A subset of Wnt/PCP molecules influence craniofacial cartilage development

(A–F) Not all identified core Wnt/PCP zebrafish mutants have a craniofacial chondrocyte stacking defect. Confocal images of whole-mount Wheat Germ Agglutanin (WGA) staining (gray) of Wnt/PCP mutant embryo heads at 4 dpf. Scale bar = 50 μm. (G-L) Confocal images of a single focal plan of WGA staining (gray) of Wnt/PCP mutant craniofacial cartilage elements at 4 dpf. Nuclei were labeled with DAPI (blue). Scale bar = 20μm. M. Graph of length to width ratio. The y-axis is all 40 chondrocyte measurements from 4 different ceratohyals for wild type and mutant genotypes. The x-axis is the length to width

ratio with a graphical representation of select ratios. The mean LWR and their respective standard deviation is marked by red cross-hairs and stated in Supplemental Table 1. To determine if data could be compared pairwise the D'Agostino and Pearson omnibus normality test was used. Mann-Whitney U was determined and the statistical significances between the means is marked on graph and stated in Supplemental Table 1. Abbreviations: M = Meckel's cartilage, CH = ceratohyal, CB = ceratobranchial, HM = hyomandibular, IH = interhyal joint, and PQ = palatoquadrate.

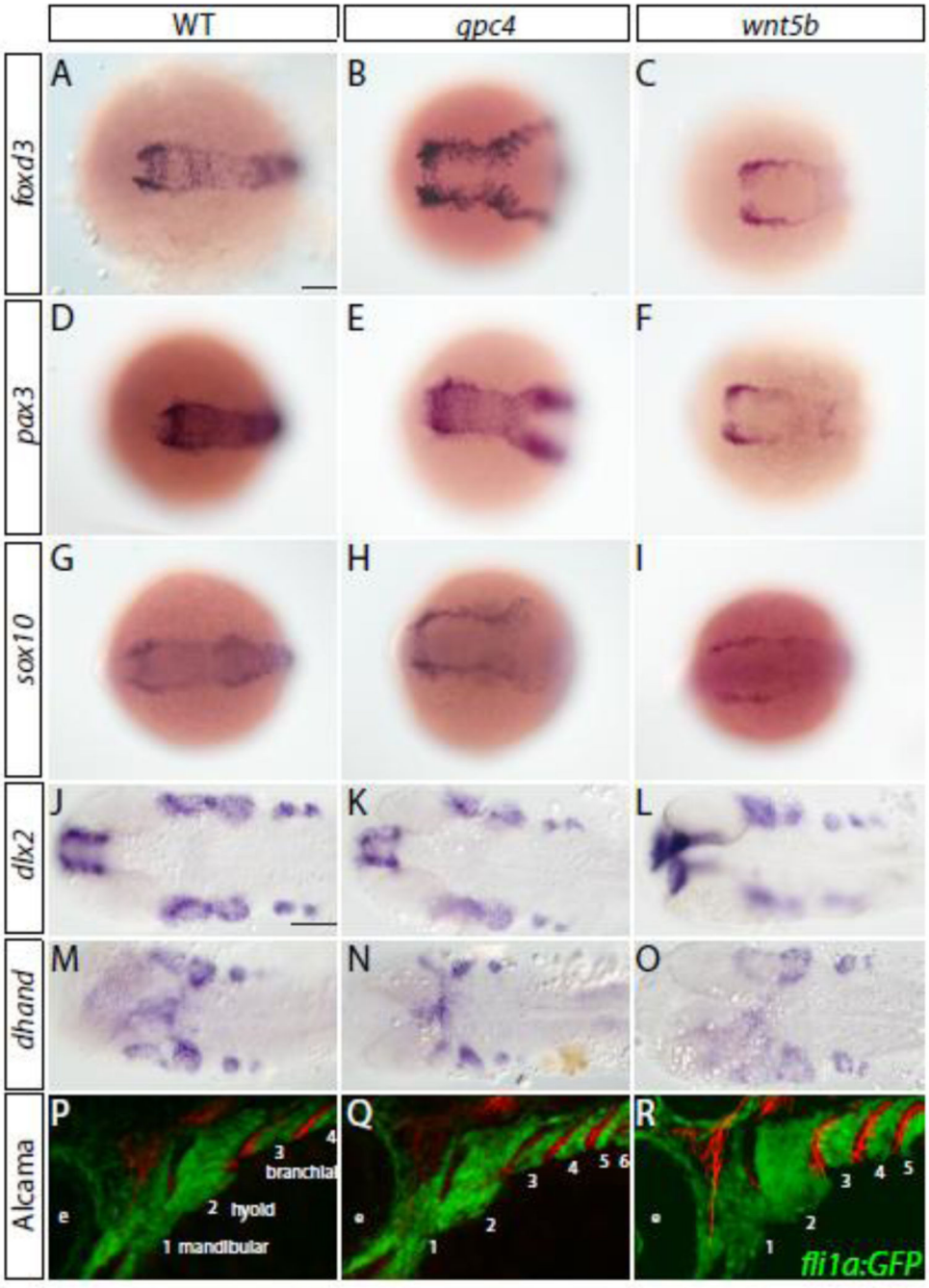

Fig. 3. Cranial neural crest cell migration and specification is unaffected in *gpc4* and *wnt5b* mutants

(A–O) Neural crest specification appears normal within *gpc4* and *wnt5b* mutants Scale bar = 100 μm. (A– I) Pre-migratory neural crest markers. 6 somites. (J–O) Pharyngeal arch markers. (J–L) 28 hpf. (M–O) 32 hpf. (P–R) Migration of neural crest appears to be unaffected in *gpc4* and *wnt5b* mutants when compared to wild type fish. *Tg(fli1a:EGFP)*^{y1} embryos have neural crest derived cells labeled by GFP expression. Embryos were fixed at

33 hpf and stained with the Alcama (Zn5) antibody (red). Pharyngeal arches are numbered. Scale bar = 50 μm.

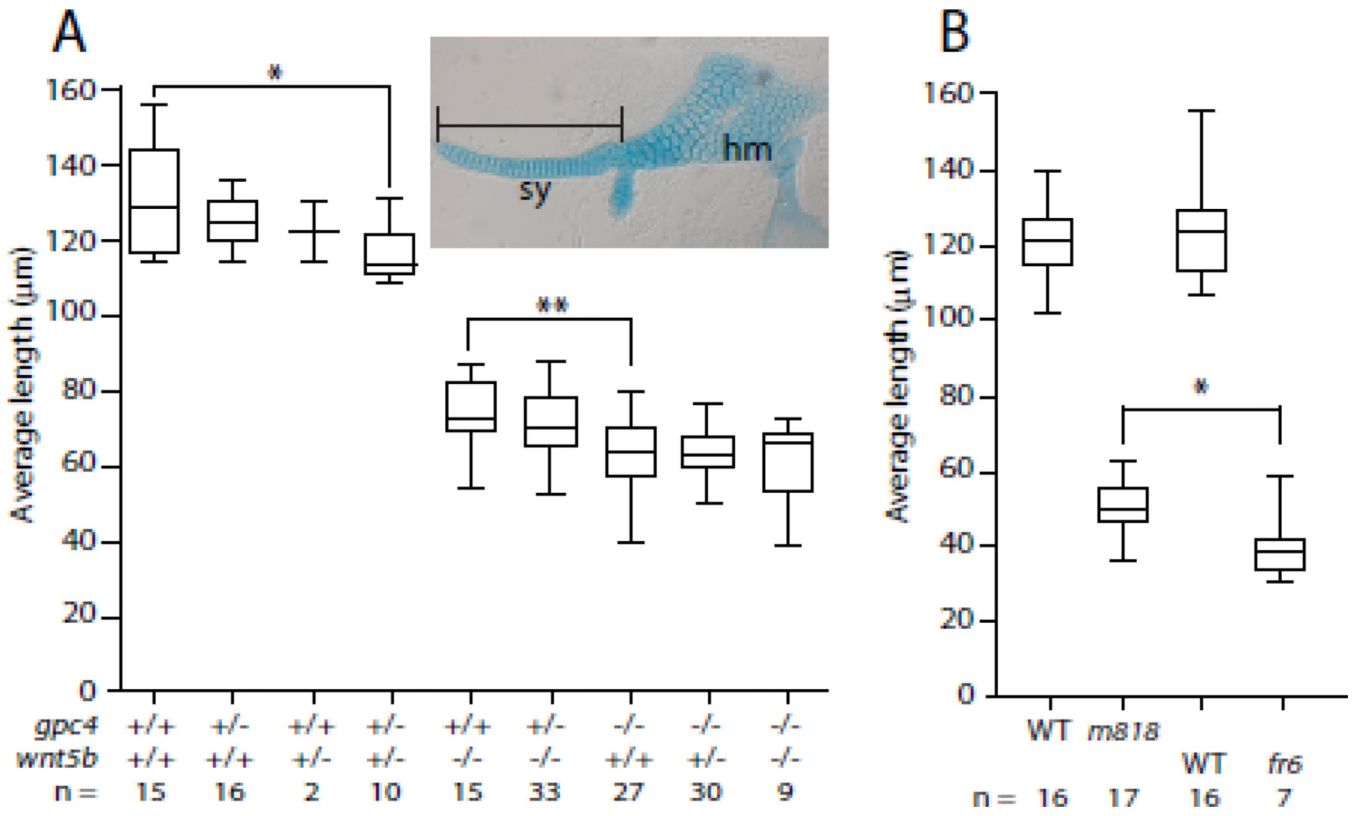

Fig. 4. The *gpc4* mutant craniofacial phenotype is not enhanced by the loss of *wnt5b*

(A–B) The length of the symplectic element (see inset) from 5 dpf embryos. (A) Measurements of the symplectics from progeny of a dihybrid cross of *gpc4*^{m818} and *wnt5b*^{ta98}. The presence of *wnt5b*^{ta98} does not enhance the *gpc4*^{m818} phenotype, but the double heterozygous mutant is significantly different than wild type. Tests of 14 *a priori* hypotheses were conducted using a Bonferroni adjusted alpha level of 0.00357 (0.05/11). * p = 0.0015, Mann-Whitney U (df) = 20. ** p = 0.0021, Mann-Whiney U (df) = 88. (B) The symplectic cartilage is significantly smaller in *gpc*^{4fr6} mutants than the symplectic elements in *gpc4*^{m818} mutants. * p = 0.0157, Mann-Whitney U (df) = 22. Abbreviations: sy = symplectic, hm = hyomandibular.

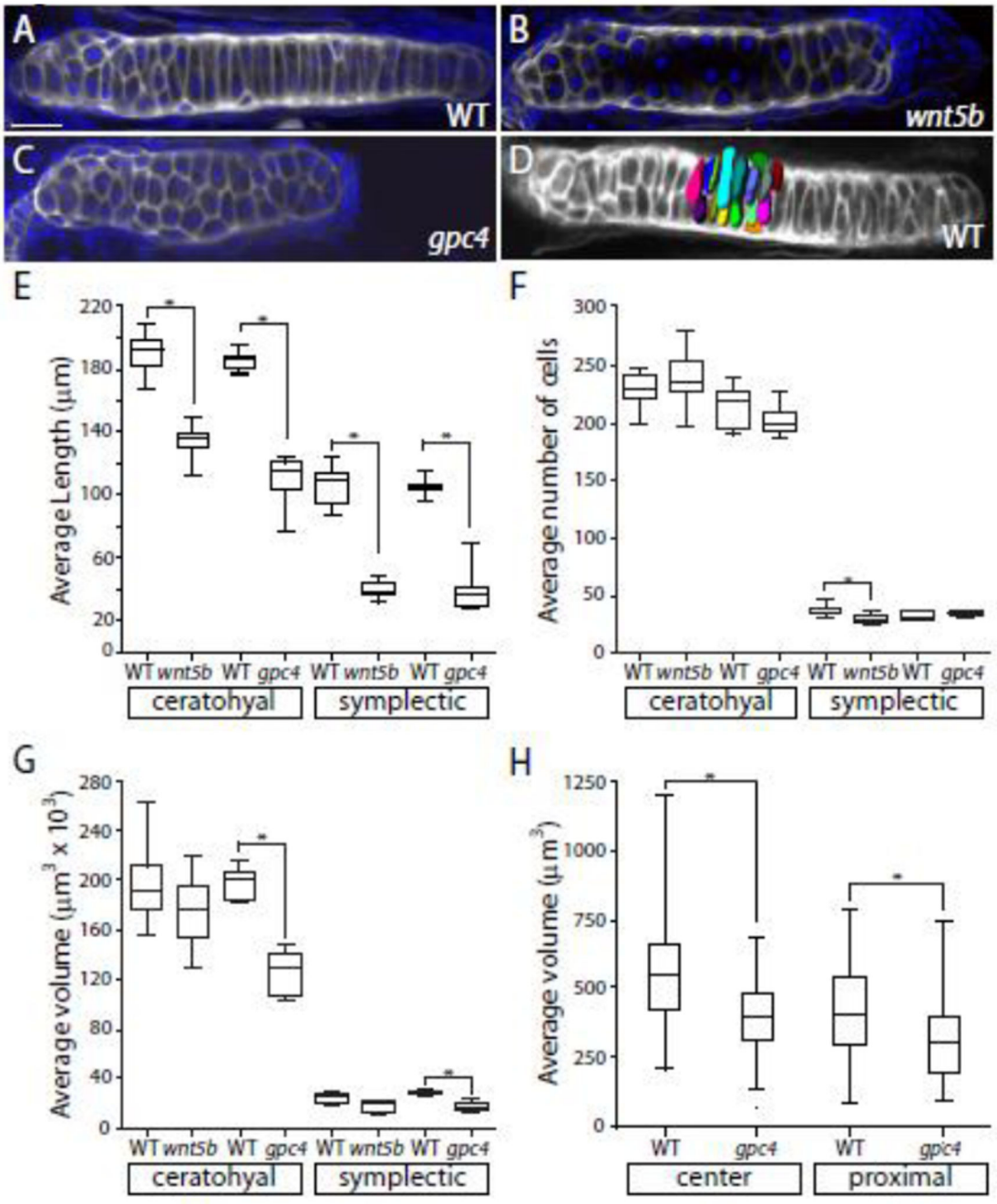

Fig. 5. Craniofacal cartilage volume is reduced in *gpc4* mutants while the numbers of cells is unchanged

(A–C) Wheat germ agglutinin (gray) and DAPI (blue) staining of ceratohyal elements. (D) A 3D reconstruction of 20 cells in the center of a wild type ceratohyal stained with WGA to determine cell volume. (E) There is a significant difference between the average length of the ceratohyal and symplectic elements between the wild type and mutants. All are p = < 0.001. (F) The average number of cells in ceratohyal and symplectic elements. (G) The average volume of the ceratohyal and symplectic elements. The ratio of the ceratohyal

element volume is $V_{fr6}/V_{WT} = 0.63$. (E–G) Tests of four *a priori* hypotheses were conducted using a Bonferroni adjusted alpha level of 0.0125 (0.05/4). * $p < 0.0125$. (H) The average volume of 20 cells in the center and proximal ends from three ceratohyal elements from *gpc4*^{fr6} embryos and their phenotypically wild type siblings. Tests of two *a priori* hypotheses were conducted using a Bonferroni adjusted alpha level of 0.025 (0.05/2). * $p < 0.025$. The ratio of the center chondrocyte volume is $V_{fr6}/V_{WT} = 0.71$. The ratio of the proximal chondrocyte volume is $V_{fr6}/V_{WT} = 0.74$. Scale bar = 20 μm.

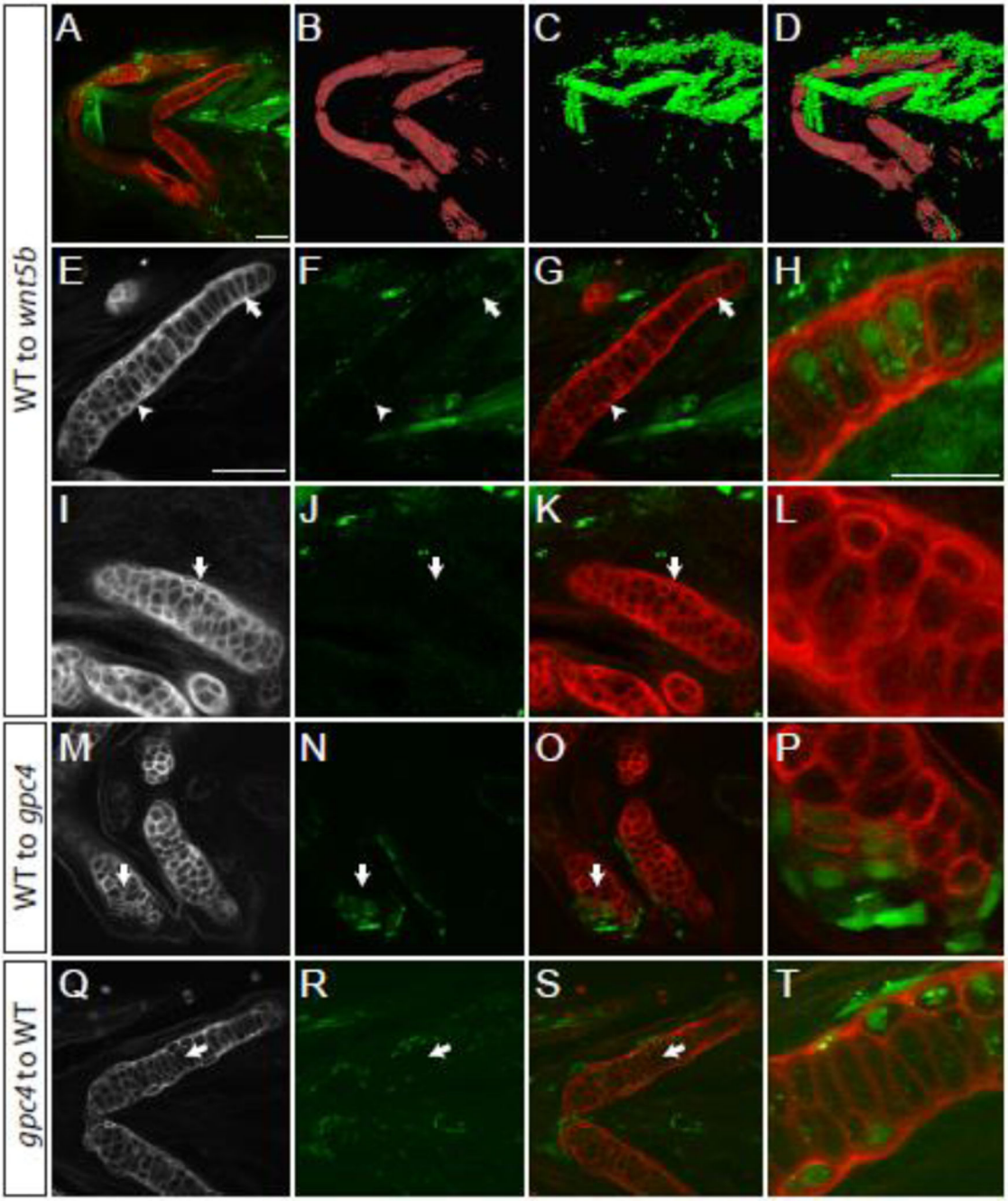

Fig. 6. In craniofacial cartilage *gpc4* acts autonomously

Transplantations to test for cell autonomy. (A–H) Transplanted wild type cells appear to rescue the *wnt5b* phenotype in the ceratohyal. (B–D) 3D reconstruction of panel A. (E–H) The ceratohyal with transplanted cells shown in A. Arrow indicates elongated transplanted cells surrounded by mesodermal transplanted cells. (H) Enlargement of area indicated in E–G by the arrow. (I–L) The certatohyal that is not transplanted with wild type cells in panel A retains its *wnt5b* phenotype. (I–K) Arrows indicate region of enlargement shown in L. (M–P) Wild type transplanted cells into a *gpc4* meckel's cartilage are cell autonomous and

elongate (arrow). (P) Enlargement of M–O at arrow. (Q–T) *gpc4* transplanted cells to a wild type host are cell autonomous and are rounder than wild type cells. (T) Enlargement of L-N at arrow. (E–Q) Wheat Germ Agglutinin (WGA) staining of ceratohyal cartilage. (F, J, N and R) Transplanted cells marked by streptavidin. (A–G, I–K, M–O, Q–S) scale bars = 50 μm. (H, L, P, T) scale bar = 25 μm. WGA (red), transplanted cells marked by Alexa-Streptavidin (green).

Table 1

Average length to width ratios (+/− SD) of ceratohyal chondrocytes

Chondrocytes	Region A	Region B	Region C
WT to WT transplants	1.65 (0.64) n = 37, p = 0.238	2.57 (1.01) n = 10, p = 0.834	2.42 (1.11) n = 27, p = 0.165
WT to WT neighbors	2.02 (0.92) n = 11	2.66 (1.13) n = 14	2.68 (1.04) n = 28
WT to *wnt5b* transplants	1.66 (0.21) n = 3, p = 0.811	1.68 (0.67) n =18, p = 0.759	2.32 (0.62) n = 18, p = 0.392
WT to *wnt5b* neighbors	1.66 (0.71) n = 10	1.65 (0.64) n = 18	2.26 (0.77) n = 21
wnt5b to WT transplants	2.13 (0.43) n = 5, p = 0.028	2.13 (1.38) n = 2, p = >0.999	1.76 (1.40) n = 6, p = 0.767
wnt5b to WT neighbors	1.48 (0.46) n = 10	2.25 (0.39) n = 7	1.83 (0.63) n = 11
WT to *gpc4* transplants	3.28 (1.61) n = 3, p = 0.934	2.32 (0.49) n=5, p = 0.0004	1.43 (0.53) n = 6, p = 0.524
WT to *gpc4* neighbors	1.39 (0.61) n = 8	1.25 (0.44) n = 16	1.56 (0.43) n = 12
gpc4 to WT transplants	1.04 (0.46) n = 44, p = <0.0001	1.21 (0.76) n = 53, p = <0.0001	1.35 (0.80) n = 26, p = 0.0002
gpc4 to WT neighbors	1.81 (0.84) n = 23	3.17 (0.86) n = 19	2.57 (0.98) n = 15

The p values indicate a comparison of the average length to width ratio of the transplanted chondrocytes to the average length to width ratio of the neighboring chondrocytes. Tests of four *a priori* hypotheses were conducted using a Bonferonni adjusted value of 0.0125 (0.05/4).